J Neurophysiol 114: 1008–1021, 2015.
First published June 10, 2015; doi:10.1152/jn.00357.2015.

Hypothalamic gonadotropin-releasing hormone (GnRH) receptor neurons fire in synchrony with the female reproductive cycle

Christian Schauer,[1]* Tong Tong,[1]* Hugues Petitjean,[1] Thomas Blum,[1] Sophie Peron,[1] Oliver Mai,[2] Frank Schmitz,[3] Ulrich Boehm,[2] and Trese Leinders-Zufall[1]

[1]*Department of Physiology and Center for Integrative Physiology and Molecular Medicine, University of Saarland School of Medicine, Homburg, Germany;* [2]*Department of Pharmacology and Toxicology, University of Saarland School of Medicine, Homburg, Germany; and* [3]*Department of Anatomy, University of Saarland School of Medicine, Homburg, Germany*

Submitted 10 April 2015; accepted in final form 9 June 2015

Schauer C, Tong T, Petitjean H, Blum T, Peron S, Mai O, Schmitz F, Boehm U, Leinders-Zufall T. Hypothalamic gonadotropin-releasing hormone (GnRH) receptor neurons fire in synchrony with the female reproductive cycle. *J Neurophysiol* 114: 1008–1021, 2015. First published June 10, 2015; doi:10.1152/jn.00357.2015.— Gonadotropin-releasing hormone (GnRH) controls mammalian reproduction via the hypothalamic-pituitary-gonadal (hpg) axis, acting on gonadotrope cells in the pituitary gland that express the GnRH receptor (GnRHR). Cells expressing the GnRHR have also been identified in the brain. However, the mechanism by which GnRH acts on these potential target cells remains poorly understood due to the difficulty of visualizing and identifying living GnRHR neurons in the central nervous system. We have developed a mouse strain in which GnRHR neurons express a fluorescent marker, enabling the reliable identification of these cells independent of the hormonal status of the animal. In this study, we analyze the GnRHR neurons of the periventricular hypothalamic nucleus in acute brain slices prepared from adult female mice. Strikingly, we find that the action potential firing pattern of these neurons alternates in synchrony with the estrous cycle, with pronounced burst firing during the preovulatory period. We demonstrate that GnRH stimulation is sufficient to trigger the conversion from tonic to burst firing in GnRHR neurons. Furthermore, we show that this switch in the firing pattern is reversed by a potent GnRHR antagonist. These data suggest that endogenous GnRH acts on GnRHR neurons and triggers burst firing in these cells during late proestrus and estrus. Our data have important clinical implications in that they indicate a novel mode of action for GnRHR agonists and antagonists in neurons of the central nervous system that are not part of the classical hpg axis.

gonadotropin-releasing hormone; hypothalamus; cetrorelix

MAMMALIAN REPRODUCTION DEPENDS on the appropriate secretion of gonadotropin-releasing hormone (GnRH). In particular, GnRH neurons in the preoptic area of the hypothalamus project to the median eminence and release GnRH into the vascular system, ensuring central control of reproduction via the hypothalamic-pituitary-gonadal (hpg) axis (Gore 2002). GnRH secretion occurs in pulses that increase in magnitude and frequency prior to ovulation (Sisk et al. 2001). To maintain fertility, secreted GnRH binds to its receptor in the pituitary to control gonadotropin release, thus regulating oocyte maturation and ovulation in both rodents and humans.

GnRH has also been implicated in the regulation of reproductive physiology, independent of gonadotropin release (Dyer and Dyball 1974; Moss 1977; Moss and Foreman 1976; Moss and McCann 1973; Pfaff 1973). Accordingly, neurons expressing the GnRH receptor (GnRHR) have been documented in multiple brain areas (Badr and Pelletier 1987; Jennes et al. 1997; Wen et al. 2011). However, the mechanism by which GnRH acts on these potential target cells in the brain remains poorly understood due to the scattered distribution of the neurons and thus our inability to reliably locate them. To overcome this problem, we have developed a genetically modified mouse strain in which GnRHR neurons express a fluorescent marker, enabling us to identify these cells independently of the hormonal status of the animal (Wen et al. 2011). Importantly, expression of the fluorescent reporter does not depend on the highly regulated *GnRHR* promoter after Cre-mediated recombination. Instead, tau green fluorescent protein (τGFP) expression is controlled by the constitutively active *ROSA26* promoter. This binary genetic approach allows a consistent identification of these neurons (Wen et al. 2011).

Interestingly, we have found GnRHR neurons in the periventricular hypothalamic nucleus (Pe), a thin region that forms a wall around the third ventricle (3V) in the rostral, intermediate, and caudal hypothalamus. Parts of this region have an ineffective blood-brain barrier (BBB) (Cottrell and Ferguson 2004; Herde et al. 2011; Saper 2004) and are thus potentially susceptible to various endogenous GnRH sources, such as GnRH-secreting neuronal fibers, 3V cerebrospinal fluid, or the cerebrovascular system (Caraty and Skinner 2008; Cottrell and Ferguson 2004; Skinner et al. 1997). If GnRH, which is elevated in the rodent median eminence during the preovulatory period (Sisk et al. 2001), is able to reach its target neurons via the vascular or 3V system, then the activity of GnRHR neurons in the periventricular nucleus should be linked to the female reproductive cycle.

We therefore investigated GnRHR neurons in acute brain slices prepared from adult female mice. We identify six novel features of hypothalamic Pe GnRHR neurons: *1*) GnRHR neurons alternate their action potential firing patterns during the female reproductive cycle; *2*) these neurons are exquisitely sensitive to subnanomolar GnRH concentrations, with $K_{1/2}$ values around 0.5 nM, initially generating a depolarizing conductance; *3*) GnRH application typically produces a short-lived response followed by longer-latency, long-lasting changes in action potential activity, and these responses are concentration dependent; *4*) GnRH stimulation seems to be the main trigger

* C. Schauer and T. Tong contributed equally to this work.

Address for reprint requests and other correspondence: Trese Leinders-Zufall, Univ. of Saarland School of Medicine, Center for Integrative Physiology and Molecular Medicine, Bldg. 48, 66421 Homburg, Germany (e-mail: trese.leinders@uks.eu).

for conversion of action potential firing mode during the preovulatory period; *5*) GnRHR neurons possess close appositions with Pe capillaries; and *6*) GnRHR neuron activity is modulated by systemic treatment with a GnRHR antagonist. These properties enable hypothalamic Pe GnRHR neurons to switch firing mode depending on fluctuations in GnRH levels during the estrous cycle, suggesting an important functional role of these neurons in female reproductive performance.

MATERIALS AND METHODS

Animals. Mouse experiments were carried out in accordance with U.S. National Institutes of Health guidelines and the German Animal Welfare Act, European Communities Council Directive 2010/63/EU, and the institutional ethical and animal welfare guidelines of the University of Saarland. Approval came from the animal welfare committee of the State of Saarland. Mice were kept under a standard light/dark cycle (12:12-h; lights-on at 07:00 h; lights-off at 19:00 h) with food and water ad libitum. GnRHR-IRES-Cre (GRIC) mice were bred with eR26-τGFP reporter mice to express τGFP in GnRHR neurons (Wen et al. 2011). The mice were kept in a mixed (129/SvJ and C57BL/6J) background.

Solutions and chemicals. Oxygenated extracellular solution S1 (95% O_2/5% CO_2) contained the following (in mM): 120 NaCl, 25 $NaHCO_3$, 5 KCl, 5 *N,N*-bis(2-hydroxyethyl)-2-aminoethanesulfonic acid (BES), 1 $MgSO_4$, 1 $CaCl_2$, and 10 glucose (300 mOsm). Extracellular S2 solution contained the following (in mM): 145 NaCl, 5 KCl, 1 $CaCl_2$, 1 $MgCl_2$, and 10 HEPES (pH 7.3, NaOH; 300 mOsm, glucose). Stock solutions of GnRH were prepared in extracellular S2 solution containing 0.1% BSA, and aliquots were stored at −20°C. GnRH was diluted in extracellular S2 solution immediately prior to use and focally applied using multibarreled stimulation pipettes. Cetrorelix, an antagonist of GnRHR (Halmos et al. 1996; Reissmann et al. 2000), was applied via microperfusion. A stock solution of cetrorelix was prepared in extracellular S2 solution, and aliquots were stored at −20°C and diluted in extracellular S2 solution immediately prior to use. Unless stated otherwise, all chemicals were purchased from Sigma (Munich, Germany).

Brain slice preparation. All experiments were performed on coronal brain tissue slices freshly prepared from female GRIC/eR26-τGFP mice (2–4 mo old) using, with slight modifications, methods described previously (Schauer and Leinders-Zufall 2012; Wen et al. 2011). Mice were anesthetized with isoflurane, followed by decapitation. The brain was quickly removed, submerged in ice-cold extracellular S1 solution, and sliced (275 μm thickness) using a vibratome (HM 650 V; Microm, Walldorf, Germany). Brain slices were obtained and analyzed between bregma +0.26 and −1.94 mm (Paxinos and Franklin 2001). As indicated previously (Wen et al. 2011), GnRHR neurons are dispersed over many brain areas, including the periventricular nucleus. However, the more rostral area (four sections between bregma 0.26 and −0.1 mm) as well as the more caudal region (four sections between bregma −1.58 and −1.94 mm) contained between zero and five GnRHR neuron somata per brain slice (~two somata/slice). Most GnRHR neurons were found in the medial region (~16 somata/slice). Their primary location has been documented between bregma −0.22 to −1.46 mm (10–30 somata/slice), and this medial periventricular area was thereby subdivided into nine separate sections according to the method described by Paxinos and Franklin (2001). Before the start of an experiment, brain slices were kept in oxygenated S1 solution (95% O_2/5% CO_2) at 31.5°C for 30 min followed by a 30-min incubation at room temperature. Brain slices were obtained during the morning of each reproductive stage, except for proestrus, during which brain slices and recordings were acquired either in the morning (early proestrus, P_E: 08:00–12:00 h) or afternoon (late proestrus, P_L: 15:00–18:00 h).

Electrophysiological recordings. Individual neurons were visualized using an Olympus BX51WI fixed-stage microscope equipped with infrared-optimized differential interference contrast (IR-DIC) optics. Slices were continuously superfused with oxygenated S1 solution (~2 ml/min; gravity flow) at room temperature. Patch pipettes (5–7 MΩ) were pulled from borosilicate glass capillaries with a filament (1.50 mm OD/0.86 mm ID; Science Products, Hofheim, Germany) on a PC-10 vertical micropipette puller (Narishige Instruments, Tokyo, Japan) and fire-polished using an MF-830 Microforge (Narishige Instruments). Action-potential-driven capacitive currents (Leinders-Zufall et al. 2007) from genetically identified neurons were recorded extracellularly using patch pipettes filled with extracellular S2 solution (seal resistance 20–90 MΩ) connected to a computerized EPC-10 patch clamp amplifier (HEKA Elektronik, Lambrecht/Pfalz, Germany). The pipette potential in the loose-patch configuration was kept at 0 mV. Spontaneous and GnRH-induced action potential discharges were monitored at a sampling rate of 10 kHz. Whole-cell current-clamp or voltage-clamp recordings were performed using the following pipette solution (in mM): 11.8 KCl, 133.2 KOH, 1 EGTA, 0.1 $CaCl_2$, 130 methanesulfonic acid, 1 Mg-ATP, 1 Na-GTP, and 10 HEPES (pH 7.2, KOH; 280 mOsm, glucose). Brain slices used for the whole-cell recordings were incubated for 15 min at 31.5°C in oxygenated *N*-methyl-D-glucamine (NMDG)-containing incubation solution (95% O_2/5% CO_2) containing (in mM): 93 NMDG, 84 HCl, 2.5 KCl, 1.2 NaH_2PO_4, 30 $NaHCO_3$, 20 HEPES, 5 Na-ascorbate, 2 thiourea, 3 Na-pyruvate, 10 $MgSO_4$, and 0.5 $CaCl_2$ (pH 7.3, HCl; 300 mOsm, glucose). The slices were then transferred into oxygenated S1 solution for 30 min at room temperature before starting to patch-clamp GnRHR neuron.

Stimuli were applied for 1 s with an interstimulus interval of 9 min. Signals were low-pass filtered (analog 3- and 4-pole Bessel filters in series), with an effective corner frequency (−3 dB) of 3.0 kHz. The electrophysiological data were analyzed using IGOR PRO software (WaveMetrics) and NeuroExplorer (Nex Technologies). A cocktail of blockers to prevent fast synaptic transmission was used in some of the loose-patch and in all the whole-cell recordings. This cocktail contained (in μM): 10 CNQX (Abcam), 50 D-AP5 (Abcam), 10 LY-341495 (Abcam), 1 CGP-52432 (Abcam), and 10 bicuculine methiodide. In whole-cell voltage-clamp recordings, 1 μM TTX was added to the cocktail of synaptic blockers. This concentration inhibited all action potential activity in neurons recorded in our slices (data not shown).

Analysis of spike data. An interspike interval (ISI) threshold for burst detection (Selinger et al. 2007) was determined (<1.3 s and at least three spikes) to facilitate calculation of the mean burst duration. The burst detection threshold was used to assist in the calculation of two other parameters: the percentage of spikes in a burst (PSiB) and the mean number of spikes in a burst (MSiB). The coefficient of ISI variation (CV_{ISI}) was calculated using the method described by Robin et al. (2009) in which the standard deviation (SD) of the ISI is divided by the mean ISI value. A hierarchical cluster analysis was combined with principal component analysis (PCA) to detect coherent patterns in the spike activities of the GnRHR neurons. The PCA was used to determine which linear combinations of *Z*-scores best explain the observed signature variation among all neurons. A hierarchical clustering algorithm, Ward's method (Origin 8.6; OriginLab, Northampton, MA), generated a partition regarding the grouping of the neurons in a multidimensional space with minimal variance. The main clusters were compared using ANOVA with Tukey's multiple comparison procedure as a post hoc comparison. Four properties (CV_{ISI}, PSiB, MSiB, and mean spike frequency and cluster) were included for each neuron. To determine changes in mean spike frequency, the spike frequency index was calculated as the ratio of the mean frequency during the first 10 s following stimulation (t_0 + 10 s) and the frequency of action potentials during the 10 s prior to stimulation (t_0 − 10 s). The parameter t_0 indicates the start of the GnRH stimulation. Similarly, the change in membrane potential (ΔV) was estimated as the ratio of mean membrane potential during the first 10 s following stimulation (t_0 + 10 s) and the mean membrane potential

during the 10 s prior to stimulation ($t_0 - 10$ s). First-spike latency was defined as the time from the stimulus onset (t_0) to the occurrence of the first action potential (Pawlas et al. 2010). The variance of the instantaneous spike frequency (VARiF) was calculated over three periods: one period prior to stimulation (Δt_C) and two periods (Δt_{G1} and Δt_{G2}) following GnRH stimulation (total recording time 180 s). The cumulative normalized variance [$V(t) = V_C(t) + V_{G1}(t) + V_{G2}(t)$] was plotted for the three periods and fitted by nonlinear regression (Origin 8.6; OriginLab) using the following equations: *1*) for Δt_C, $V_C(t_{-1},t_0) = s1 \cdot t + a$; *2*) for Δt_{G1}, $V_{G1}(t_1,t_2) = s2 \cdot t + b$; and *3*) for Δt_{G2}, $V_{G2}(t_2,t_3) = s3 \cdot t + c$.

Slope s1 provides an estimate of the mean variance prior to GnRH stimulation (control) and *slope s2* indicates the mean variance following GnRH stimulation. *Slope s3* is a measure of the return of the mean variance to prestimulation (control) values: $0.9 \cdot s1 < s3 < 1.1 \cdot s1$. The time t_0 marks the start of GnRH stimulation. The parameter t_{-1} indicates the start of recording, t_1 is the time at which GnRH induces a change in variance, and t_2 is the time at which the variance returns to control levels. A 20% change in variance ($0.8 \cdot s1 < s2 > 1.2 \cdot s1$) for at least 5 s indicated a GnRH-induced modification in the spike code. The determination coefficient of the regression was always >0.98. The parameters t_1 and t_2 help determine the length of latency ($L_G = t_1 - t_0$) and the duration of GnRH-induced long-lasting conversion in spike activity ($D_G = t_2 - t_1$).

Cytological assessment of the reproductive stage. A vaginal smear was obtained by vaginal washing (Caligioni 2009). A glass fire-polished Pasteur pipette filled with 10 μl of PBS was placed into the vagina of the mouse. The vagina was gently flushed three to five times. The PBS containing the vaginal secretion was placed on a slide and examined under a microscope. The stage of the estrous cycle was determined by identifying the cell types and their relative quantities. Images of the vaginal smears were collected and stored with a unique identifier for the mouse on a computer and reassessed by an independent second investigator.

Immunohistochemistry. Female mice in early proestrus were anesthetized using isoflurane in the morning, followed by decapitation. The brain was quickly removed, submerged in ice-cold extracellular S1 solution, and fixed using PBS containing 4% paraformaldehyde for 2 h at 4°C. The fixed brain was sliced into 100-μm sections using a vibratome (Pelco 101; Technical Products International) prior to blocking and antibody application. The primary antibodies were anti-GFP (AB13970, 1:1,000, chicken monoclonal; Abcam) (Leinders-Zufall et al. 2014), anti-GnRH (20075, 1:800; Immunostar), and anti-CD31 (1:750, rat monoclonal; Abcam) (Schmidt and von Hochstetter 1995). The secondary antibodies were Alexa-Fluor 488 goat-anti-chicken (A-11039, 1:1,000, Invitrogen), Alexa-Fluor 488 donkey-anti-rat (A-21208, 1:1,000, Invitrogen), Alexa-Fluor 633 donkey-anti-rat (20137, 1:1,000; Biotium), and Alexa-Fluor 633 goat-anti-rabbit (A-21070, 1:1,000; Invitrogen). The procedures were conducted at room temperature, except for incubation with primary antibodies (4°C). The primary antibodies were diluted in blocking solution containing 0.5% Triton X-100 and 4% normal horse serum in PBS. Primary antibodies were incubated for 48 h, and with secondary antibodies for 90 min. Controls omitting the primary antibody did not yield any staining. Fluorescence images were acquired on either a BX51WI attached to a Radiance Confocal Laser Scanning System (Carl Zeiss AG, formerly Bio-Rad) or an LSM 710 confocal microscope (Zeiss). Image stacks are presented as maximum intensity projections, assembled, and minimally adjusted for brightness using Adobe Photoshop CS6 (Adobe Systems, San Jose, CA).

Electron microscopy. Embedding of the coronal brain slices for electron microscopy was performed as previously described (Schoch et al. 2006). Ultrathin sections were analyzed with a Tecnai Biotwin 12 digital electron microscope.

In vivo cetrorelix experiment. Female mice received subcutaneous injections of either 0.9% sodium chloride (sham group), or 10 μg or 50 μg of cetrorelix dissolved in 0.9% sodium chloride in the morning. One group of females did not receive any treatment but was analyzed in early proestrus for uterus weight and ovary status. Independent of the treatment group, the estrous cycles of the females were determined using vaginal smears. On *day 9* of the treatment, the mice were weighed and then anesthetized using isoflurane, followed by decapitation. The brain of each mouse was quickly removed for loose-patch recordings of GnRHR neurons. The uteri were dissected and weighed to calculate the uterus-to-body-mass ratio, and the ovaries were extracted for histological examination.

Staining with hematoxylin and eosin. Both ovaries from 21 females (sham, and those treated with 10 μg and 50 μg of cetrorelix, control early proestrus) were fixed in PBS containing 4% paraformaldehyde overnight at 4°C, followed by incubation in PBS containing 30% sucrose, also overnight at 4°C. Cryosections (16 μm) were stained with hematoxylin and eosin by standard procedure. Sections were immersed in hematoxylin solution for 1 min, rinsed, immersed in eosin for 1–2 min, rinsed, dehydrated using an ascending series of alcohol solutions, cleared with xylene, and finally, coverslips were placed over them. Sections were analyzed by an investigator who did not have knowledge of the treatment.

Statistical analysis. Statistical analysis was performed with GraphPad PRISM (GraphPad Software, San Diego, CA) or SPSS (IBM, New York, NY). A Student's *t*-test was used to measure the significance of the differences between two distributions. Multiple groups were compared using one-way or two-way ANOVA. Tukey's multiple comparison test or Fisher's least significant difference (LSD) was used as a post hoc comparison of the ANOVA. The probability of error level (alpha) was chosen to be 0.05. Unless otherwise stated, data are expressed as means ± SE.

RESULTS

Cyclic transformation of GnRHR neuron activity in synchrony with the estrous cycle. We first investigated the spontaneous activity of GnRHR neurons in the female mouse brain. To visualize GnRHR neurons, we bred GnRHR-IRES-Cre (GRIC) mice with eRosa26-τGFP reporter mice. The resulting GRIC/eR26-τGFP animals carry a mutant *GnRHR* allele, from which GnRHR and Cre recombinase are independently translated and specifically express τGFP under the control of the enhanced *Rosa26* promoter in GnRHR neurons (Wen et al. 2011). Previous calcium imaging experiments demonstrated that the genetically labeled neurons in these animals express a functional GnRHR (Wen et al. 2011). GRIC/eR26-τGFP females exhibited regular estrous cyclicity (Fig. 1*A*). Because endogenous GnRH secretion fluctuates during the female reproductive cycle, we recorded GnRHR neuron firing at different stages of the estrous cycle (metestrus, diestrus, proestrus, and estrus) using a combination of fluorescence and IR-DIC illumination, and extracellular loose-patch recordings (Fig. 1*B*) (Leinders-Zufall et al. 2007).

GnRHR neurons ($n = 94$) located in the Pe from 54 gonadally intact GRIC/eR26-τGFP females exhibited spontaneous spike activity (Fig. 1*C*). Neurons generally showed burst firing patterns (periods with a high action potential firing rate separated by periods of lower activity) during metestrus (M), diestrus (D), and estrus (E), but exhibited diverse firing patterns during proestrus (early proestrus, P_E; and late proestrus, P_L). Because the preovulatory GnRH surge progresses during the afternoon of proestrus (Sisk et al. 2001), we recorded GnRHR neuron activity in brain slices obtained either in the morning (P_E) or afternoon (P_L) of that stage. Regular tonic firing seemed to occur primarily during P_E (Fig. 1*C*). The mean

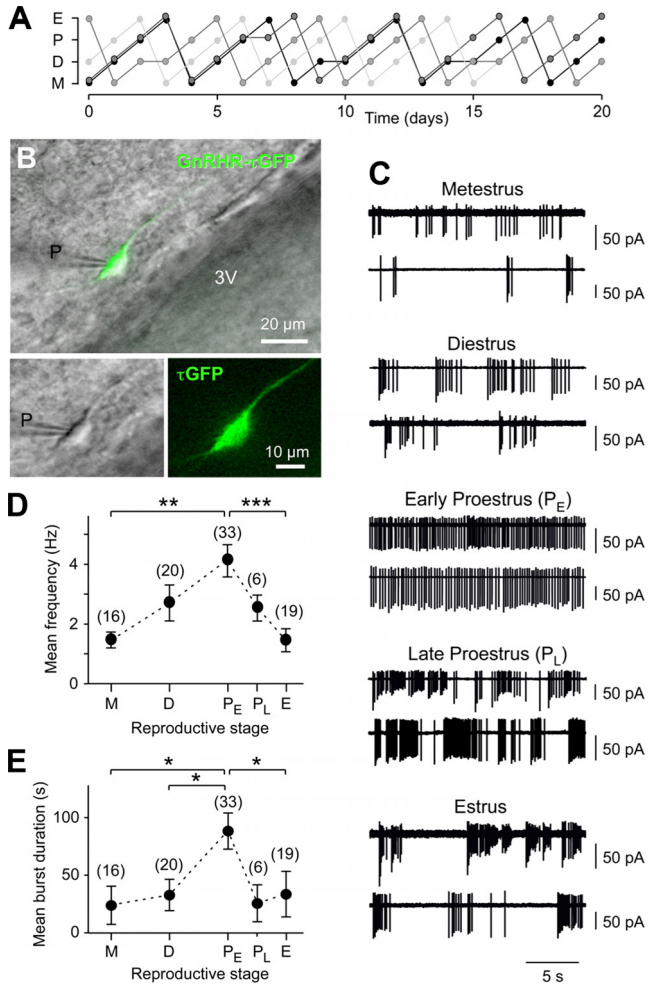

Fig. 1. The spontaneous spike activity patterns of gonadotropin-releasing hormone receptor (GnRHR) neurons change during the reproductive cycle. *A*: representative plot of the estrous cycle from four GRIC/eR26-τGFP mice (indicated with different line colors). The females display a normal cycle length of 4.5 ± 0.2 days ($n = 6$). M, metestrus; D, diestrus; P, proestrus; E, estrus. *B*: overlay of a fluorescence image on top of an infrared-differential interference contrast (IR-DIC) micrograph of a brain tissue slice identifying a GnRHR neuron in the periventricular hypothalamic nucleus (Pe), which is located next to the third ventricle (3V). The soma of the GnRHR neuron is clearly visible in the IR-DIC image (*lower left*) and expresses tau green fluorescent protein (τGFP) (*lower right*) after cre-mediated excision of a transcriptional stop sequence dependent on the activation of the *GnRHR* promoter. P, patch electrode. *C*: example recordings of trains of extracellularly recorded, action-potential-driven capacitive currents of 10 different GnRHR neurons (two different neurons per reproductive stage). The pipette potential was 0 mV. Neuronal activity during proestrus was recorded in brain slices obtained either in the morning [early proestrus, P_E (08:00–12:00 h)] or afternoon [late proestrus, P_L (15:00–18:00 h)]. *D*: the mean spike frequency of GnRHR neurons changes during the estrous cycle (ANOVA $F_{4,89} = 6.137$, $P < 0.001$), peaking at P_E. M, 1.3 ± 0.2 Hz; D, 2.5 ± 0.6 Hz; P_E, 4.0 ± 0.5 Hz; P_L, 2.2 ± 0.5 Hz; E, 1.2 ± 0.3 Hz. Tukey's test ***$P < 0.001$, **$P < 0.01$. The number of neurons recorded is shown in brackets. *E*: the mean burst duration of GnRHR neurons depends on the reproductive cycle (ANOVA $F_{4,89} = 3.962$, $P < 0.01$), with a pronounced peak during P_E. M, 19.8 ± 13.4 s; D, 29.8 ± 12.4 s; P_E, 85.9 ± 15.5 s; P_L, 21.4 ± 13.7 s; E, 27.0 ± 15.6 s; Tukey's test *$P < 0.05$. The number of neurons recorded is shown in brackets.

spike frequency revealed a cyclicity in action potential firing during the different reproductive stages that increased to 4.0 Hz during P_E compared with 1 Hz during M and E (Fig. 1*D*). Firing rate was not correlated with the seal resistance and there was no indication of a relationship between the two parameters during the various stages of the cycle (Pearson's *r*: M, $r = -0.028$, $P = 0.89$; D, $r = -0.067$, $P = 0.71$; P_E, $r = -0.092$, $P = 0.55$; P_L, $r = 0.053$, $P = 0.85$; E, $r = 0.072$, $P = 0.71$). Periods of low spike activity are known to occur mainly in neurons firing in bursts due to the long quiet periods between bursts, causing a reduction in the mean spike frequency. High mean spike frequency values, as were observed during P_E, could therefore point to a higher amount of tonically firing neurons in this stage. Because action potential firing patterns differ substantially from each other, we developed a quantitative approach to analyze the firing patterns in an unbiased manner. In the first step, an ISI threshold for burst detection was determined to facilitate the calculation of the mean burst duration. Here, a high mean burst duration is indicative of the presence of tonically firing neurons. Theoretically, tonically firing neurons should have one long burst that lasts the entire recording time due to their low ISI value and will lack the quiet periods characteristic of burst firing. A low mean burst duration, which signifies short bursts of action potential activity, indicates the presence of primarily burst firing neurons. This type of activity was detected in all stages of the reproductive cycle, with the exception of P_E (Fig. 1*E*), suggesting that hormonal input such as GnRH influences the firing pattern of these neurons. In the second step, the burst detection threshold was used to assist in calculating two other parameters: the percentage of spikes in bursts (PSiB) and the mean number of spikes in a burst (MSiB). The ISI was computed to establish the coefficient of ISI variation (CV_{ISI}; see MATERIALS AND METHODS). We then made use of PCA combined with hierarchical cluster analysis to extract relevant characteristics with which to categorize the action potential patterns (Fig. 2, *A* and *B*). This analysis technique decomposes an array of numerical data into a set of orthogonal vectors called principal components. All parameters describing the firing pattern of an individual neuron were included to compute PCA scores, which were plotted on a two-dimensional (2-D) plane defined by the first and second PCA components. A correlation circle in the PCA dataset indicates that multiple components are necessary to classify the GnRHR neurons. Using a cluster analysis to sort neurons that were sufficiently similar to each other in a multidimensional space (Ward's method with squared Euclidean distance), threshold values of the two principal components, PSiB and CV_{ISI}, were established using the divergence at the dendrogram nodes. Tonically firing neurons were recognized by a $CV_{ISI} < 0.8$ (subbranch 1); bursting and irregularly firing neurons, both having a $CV_{ISI} > 0.8$, were distinguished by a PSiB >80% (subbranch 3) and a PSiB <80% (subbranch 4), respectively. Using these criteria, we identified 33% of the neurons as tonically firing, 55% as firing in a burst pattern, and only 12% as firing irregularly (Fig. 2, *C–E*). Because irregularly firing neurons ($n = 11$) are rarely found at any stage during the reproductive cycle, they were excluded from further analysis. The distribution of tonic and bursting GnRHR neurons during the female reproductive cycle indicates that tonically firing GnRHR neurons are virtually absent during metestrus (1 out of 13 cells; Fig. 2*F*). Their quantity increased steadily to a maximal value of 63% (20 out of 32 cells) during P_E but dropped dramatically down to an occasional tonic GnRHR neuron measured during P_L (1 out of 5 cells) or estrus (2 out of 15 cells). A similar but inverse cyclicity was observed for bursting GnRHR neurons, with most being observed during

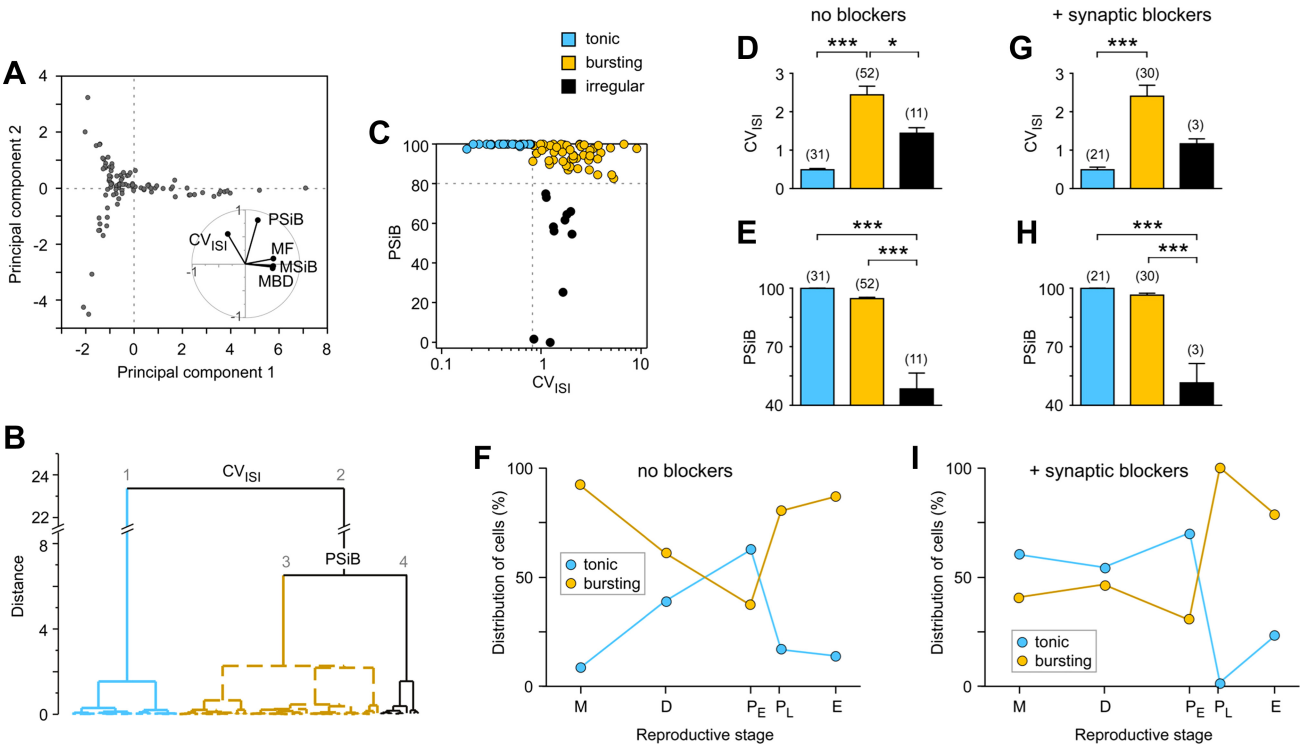

Fig. 2. GnRHR neurons alternate between tonic and bursting spike activity during the reproductive cycle. *A*: principal component analysis (PCA) was used to identify which features describe GnRHR neuron spike activity (CV_{ISI}, coefficient of variation of the interspike interval; PSiB, percentage of spikes in bursts; MSiB, mean number of spikes in a burst; MF, mean spike frequency; MBD, mean burst duration) and could enable the categorization of neurons using linear combinations of *Z*-scores. A correlation circle of the PCA dataset (*inset*) provides a projection of these variables in the factor's space and demonstrates that multiple variables of the spike activity are needed to categorize the neurons. *B*: dendrogram of individual GnRHR neurons using Ward's clustering algorithm with Euclidean distances. The first partition in the dendrogram, which separates tonic from nontonic firing neurons, is determined by significant differences in CV_{ISI}, giving mean values of 0.5 ± 0.03 (n = 31) and 2.3 ± 1.9 (n = 63) for clusters 1 and 2, respectively [t-test t(92) = 5.26, $P < 0.0001$]. The next partition within cluster 2 distinguishes neurons firing in bursts from irregularly firing neurons and is defined on the basis of PSiB having a mean value of 95.1 ± 0.7 (n = 52) and 48.7 ± 8.3 (n = 11) for clusters 3 and 4, respectively [t-test t(61) = 40.87, $P < 0.0001$]. *C*: distribution of GnRHR neurons plotted in a two-dimensional space using the PSiB and CV_{ISI} values of each recorded GnRHR neuron (n = 94). Depending on the threshold values (dashed lines) determined from the cluster analysis (see text), the neurons were categorized as firing tonically (*blue*), in a burst pattern (*yellow*), or irregularly (*black*). *D* and *E*: values of CV_{ISI} (*D*) and PSiB (*E*) depending on the spike activity classification of the GnRHR neurons (ANOVA $F_{2,91}$ = 25.82, $P < 0.001$ and $F_{2,91}$ = 120.8, $P < 0.001$, respectively). *D*: neurons firing in bursts are distinguishable from both tonic and irregularly firing neurons due to their high CV_{ISI} value (tonic, 0.49 ± 0.03; bursting, 2.44 ± 0.22; irregular, 1.44 ± 0.14). *E*: GnRHR neurons with irregular spike activity can be distinguished on the basis of their significantly different PSiB values (tonic, 99.88 ± 0.08%; bursting, 95.07 ± 0.66%; irregular, 48.72 ± 8.72%). *F*: plot of the distribution of all GnRHR neurons (n = 94) firing either tonically (*blue*) or in a burst (*yellow*) by reproductive stage. *G* and *H*: values of CV_{ISI} (*G*) and PSiB (*H*) depending on the spike activity classification of GnRHR neurons in the presence of synaptic blockers (ANOVA $F_{2,51}$ = 19.04, $P < 0.0001$ and $F_{2,51}$ = 120.2, $P < 0.0001$, respectively). *G*: neurons firing in bursts are distinguishable from tonically firing neurons because of their high CV_{ISI} values (tonic, 0.50 ± 0.04; bursting, 2.43 ± 0.27; irregular, 1.17 ± 0.15). *H*: GnRHR neurons with irregular spike activity can be distinguished on the basis of their significantly different PSiB values (tonic, 99.92 ± 0.05%; bursting, 96.59 ± 0.92.%; irregular, 51.54 ± 9.83%). *I*: plot of the distribution of all GnRHR neurons (n = 54) firing either tonically (*blue*) or in a burst (*yellow*) by reproductive stage, in the presence of synaptic blockers. M, metestrus; D, diestrus; P_E, early proestrus; P_L, late proestrus; E, estrus. Tukey's test ***$P < 0.0001$, *$P < 0.05$. The number of neurons is plotted in brackets above each bar.

metestrus (12 out of 13 cells, 92%). The number of bursting neurons declined over the following stages to a low of 12 out of 32 cells (37%) and dramatically increased again on the day of estrus (13 out of 15 cells, 87%).

To exclude synaptic input onto GnRHR neurons as the cause for the change in the amount of tonic vs. burst firing neurons during the reproductive cycle, we repeated the experiments in the presence of synaptic blockers (Fig. 2. *G–I*). A similar distribution of tonic, bursting, and irregular firing neurons was observed: 39% fired tonically, 55% fired in a burst pattern, and only 6% fired irregularly (Fig. 2, *G* and *H*). The properties of the neurons (e.g., CV_{ISI}, PSiB, and mean spike frequency) were indistinguishable from those of GnRHR neurons in the absence of synaptic blockers (P = 0.16–0.87). However, the distribution of tonic and bursting GnRHR neurons during the female reproductive cycle was considerably reorganized (Fig. 2*I*). A rise in bursting GnRHR neurons appeared to depend on the preovulatory period starting in P_L of the reproductive cycle. No tonic firing neurons could be detected during this reproductive phase. Thus the network dampened the occurrence of burst firing GnRHR neurons during the preovulatory period. In contrast, the ratio of tonic to bursting neurons during metestrus indicates that the network enhanced the presence of burst-firing neurons (Fig. 2, *F* and *I*). These results suggest that state- (or hormone)-dependent network pathways influence the neuronal activity of GnRHR neurons in this hypothalamic region.

Taken together, the experiments demonstrate a cyclic transformation of GnRHR neuron activity that occurs in synchrony with the estrous cycle, particularly during the proestrus stage, when pronounced changes in GnRH concentration have been measured in the median eminence of rodents (Sisk et al. 2001).

GnRH is sufficient to trigger the switch in action potential burst activity in Pe GnRHR neurons. We hypothesized that GnRH itself could be responsible for the conversion from tonic to burst firing in GnRHR neurons. To establish whether GnRH directly affects the τGFP-tagged neurons, we first recorded GnRH-induced responses in the presence of synaptic blockers during P_E (Fig. 3, *A–E*). Without interfering with the composition of the cytoplasm, GnRH increased the spike frequency within the first 10 s following GnRH stimulation, from 5.0 ± 1.3 to 6.8 ± 1.3 Hz ($P < 0.05$; Fig. 3, *A* and *B*). Under current-clamp, GnRH had a significant effect on both the membrane potential and spike frequency (Fig. 3, *C*–E). A 1-s pulse of 1 nM GnRH induced an initial action potential burst followed by an extended elevation of the membrane potential (Fig. 3*C*). The GnRH-induced depolarization ranged from 0.5 to 3.2 mV, depending on the resting membrane potential, which was −49.5 ± 2.7 mV ($n = 5$) on average. Resting membrane potential refers to 0-pA current injection. A trend by which a more negative resting membrane potential produces a higher depolarization was observed (Pearson's $r = -0.8$). The spike frequency within the first 10 s following GnRH stimulation increased approximately by a factor of 2 (Fig. 3*E*). Thus the whole-cell recordings in the presence of synaptic blockers, which isolated the GnRHR neurons from fast neurotransmitters at presynaptic specializations, suggest that GnRH is the initial activator of a change in membrane excitability through either the activation of a depolarizing conductance or the inhibition of a hyperpolarizing conductance. To further isolate GnRHR neurons from the network and to prevent spontaneous action potentials to release dense-core vesicles, we performed whole-cell voltage-clamp experiments in the presence of synaptic blockers and the sodium channel toxin TTX. Under these circumstances we observe an inward current having an amplitude of −2.16 ± 0.94 pA ($n = 5$) at −60 mV in the presence of 10 nM GnRH (Fig. 3, *F–H*) demonstrating a direct effect of GnRH on GnRHR neurons. We cannot exclude the existence of combinative current mechanisms, because neurons have the ability to produce stereotyped physiological action potential patterns with variable underlying membrane conductances (Marder et al. 2014). Our results do, however, point out that GnRH directly affects τGFP-labeled neurons, establishing that the neurons contain functional GnRHR.

To avoid inadvertently impairing the fundamental neural mechanisms that influence the activity of the GnRHR neurons by disrupting neurotransmission and to imitate a more natural environment, we refrained from using synaptic blockers in further experiments. GnRHR neurons firing tonically during P_E showed a similar mean spike frequency in the absence of a synaptic blocker cocktail (0.47 ± 0.04 Hz, $n = 20$) as when the cocktail was present [0.53 ± 0.09 Hz, $n = 7$; $t(25) = 0.79$, $P = 0.43$]. GnRHR neurons stimulated with GnRH also responded with a rise in spike frequency and, within a certain concentration range, a higher GnRH concentration elicited a higher increase in mean spike frequency, with a $K_{1/2}$ value of 0.62 ± 0.13 nM (Fig. 3, *I* and *J*; ANOVA $F_{4,74} = 2.15$, $P < 0.01$). We next examined the timing of the first spike following GnRH stimulation to determine whether any spatio-temporal pattern for GnRH-induced change occurs in the initial action potential sequence. Independent of the noise caused by spontaneous action potential activity, we found a dose-dependent change in the first-spike latency (Fig. 3*K*). With increasing GnRH concentration, the latency decreased from a value of 340 ms at 0.1 nM to ~60 ms at 10 nM GnRH. A hormonal modulation of behaviors likely relies on neural firing over extended periods. Intriguingly, GnRHR neurons showed long-lasting changes in spike activity in response to a 1-s GnRH stimulation that persisted for 1–2 min at saturating 10 nM GnRH, in addition to the short-lived responses (Fig. 3, *L–O*). To use our tools for distinguishing the tonic and burst firing patterns, recordings of at least 3.5 min are required, which go beyond the changes induced by a 1-s pulse. The variance in action potential activity appears to be an essential feature of classifying tonic vs. bursting neurons since the CV_{ISI} is the most important factor differentiating the spike patterns. Therefore, we analyzed the cumulative VARiF, and 0.1 nM GnRH did not alter the firing pattern (VARiF control, 0.23 ± 0.11, $n = 21$; 0.1 nM GnRH, 0.19 ± 0.10, $n = 9$; *t*-test $P = 0.27$). From 0.3 up to 10 nM GnRH, both the duration and latency in spike activity conversion increased significantly (Fig. 3, *N* and *O*) (duration: 0.3 nM: 10.6 ± 1.1 s, $n = 16$; 10 nM: 29.9 ± 1.8 s, $n = 4$; latency: 0.3 nM: 27.2 ± 5.9 s, $n = 16$, 10 nM: 77.7 ± 18.5 s, $n = 4$; Tukey's test $P < 0.01$). Both dose-dependent properties were fitted with a Hill equation, giving $K_{1/2}$ values (mean ± SD) of 0.46 ± 0.17 and 0.48 ± 0.11 nM for the duration and latency of the long-lasting conversion in spike activity, respectively. All $K_{1/2}$ values (Fig. 3) were in close proximity to one other and to values published for GnRHR in cultured pituitary and immortalized gonadotrope-like cells (Barran et al. 2005; Conn and Hazum 1981; Lu et al. 2005), thus implying that the observed modulations in spike activity occurred due to activation of the receptor itself. Our results demonstrate that GnRH can act as a strong modulator of the firing activity of GnRHR neurons. The long-lasting change in VARiF following a short pulse of GnRH could be a first indication of the initiation of action potential plasticity leading to the transformation from a tonic to a burst or irregular firing pattern.

To explore the possibility that GnRHR neurons can alter their firing patterns for a prolonged period with sustained GnRH stimulation, we assessed the action potential firing of tonic GnRHR neurons from females during P_E stimulated with 10 nM GnRH for 10 min up to 1½ h (Fig. 3, *P–S*). During these recordings, the mean firing frequency and the two parameters of spike code classification (CV_{ISI} and PSiB) were evaluated every 220 s (Fig. 3*Q*). All tonically firing GnRHR neurons had a basic CV_{ISI} <0.8 and a PSiB of 99.8 ± 0.21 ($n = 6$). The mean spike frequency decreased and the characteristic parameter CV_{ISI} increased after a 10 min of GnRH perfusion without significantly changing the PSiB (77.1 ± 33.2, $n = 6$, *t*-test $P = 0.17$), thus leading to the reclassification of the initially tonically firing GnRHR neurons as bursters. Therefore, GnRH stimulation is sufficient to trigger the switching of the mode of activity of GnRHR neurons from tonic to burst firing.

Endogenous GnRH converts the mode of GnRHR neuronal activity. If transitions to burst firing depend on endogenous GnRH receptor activation, GnRHR neuron bursting should shift to tonic firing with inhibition of GnRHR. To test this, we repeated the previous experiment in the presence of the competitive GnRHR antagonist cetrorelix (Reissmann et al. 2000). Indeed, we found that cetrorelix treatment reversed the GnRH-induced burst firing of GnRHR neurons (Fig. 4, *A–D*). As previously observed, stimulation of tonic firing by GnRH

reduced the mean spike frequency and increased the CV_{ISI}, causing reclassification of the neurons as bursters. A subsequent cetrorelix treatment converted the firing pattern back to its original state, causing the neurons to be labeled once more as tonically firing. It thus appears that the activity of GnRHR regulates the neuronal spike code. This would suggest that the burst firing of GnRHR neurons during estrus, metestrus, and diestrus (Fig. 2) could be triggered by the presence of GnRH. To test this, the spike firing activity of GnRHR neurons during the various stages of the estrous cycle was examined prior to (control) and after cetrorelix treatment in our brain slices (Fig. 4, *E–H*). Idle GnRHR activity, as predicted for tonically firing neurons during P_E, was not expected to be affected by the antagonist. Surprisingly, cetrorelix treatment reduced the CV_{ISI} value even further, indicating that low, pulsatile GnRH release may have activated GnRHR or that GnRHR, a G protein-coupled receptor (GPCR), shows agonist-independent activity that can be prevented by the antagonist. Cetrorelix exposure during estrus abolished the burst firing pattern, basically neutralizing any GnRH-induced activity (Fig. 4*G*). In comparison, the data collected during metestrus and diestrus significantly modified the action potential firing (Fig. 4*H*) but did not reduce the CV_{ISI} values below the threshold for reclassifying the neurons as tonically firing. The GnRHR activity during these two stages of the reproductive cycle is therefore not the sole driver inducing burst activity. Nonetheless, during late proestrus and estrus, our results imply that endogenous GnRH acting on the GnRHR could be the main trigger for burst firing in these neurons.

Possible sources of GnRH. Presynaptic GnRH as well as GnRH present in the 3V cerebrospinal fluid or in the vascular system could potentially stimulate GnRHR neurons. GnRH-secreting fibers appear to have no immediate contact with GnRHR neurons in the Pe. We evaluated 26 GnRHR neurons

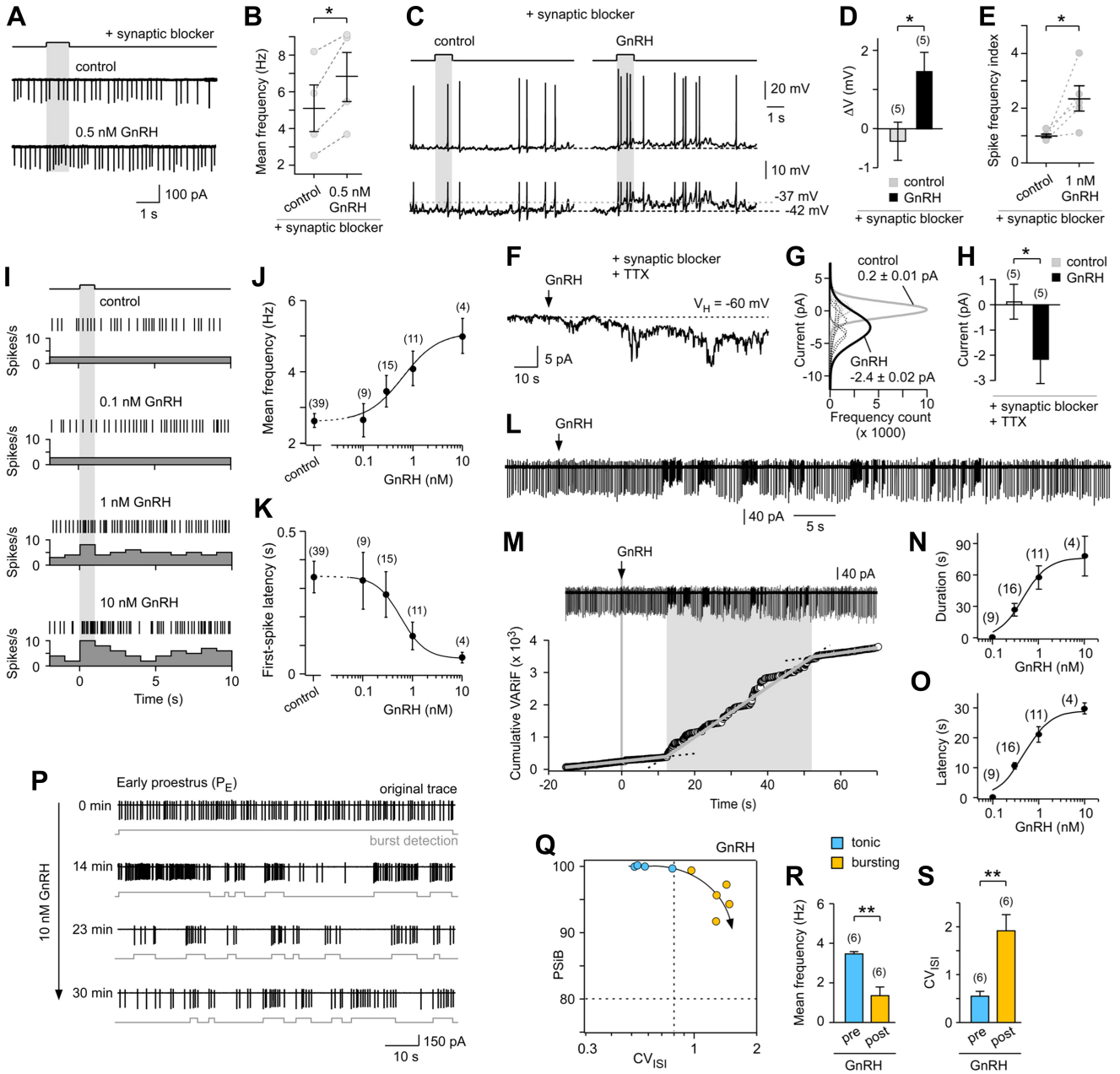

in six coronal brain slices of the medial region of the Pe (bregma −0.22 to −1.26 mm) in three early proestrus female mice and did not encounter any potential contact points (appositions <0.3 μm) between GnRH-expressing fibers and GnRHR neurons (Fig. 5*A*). In contrast, appositions between GnRH fibers and GnRHR neurons were easily identified in the arcuate nucleus (Fig. 5*B*). Both GnRH-secreting and GnRHR-expressing fibers possess branches of extensive length. Therefore, synaptic input from GnRH-secreting neurons onto Pe GnRHR neurons cannot be excluded entirely.

GnRH diffusion from either the 3V or the vasculature could offer an alternative option for the regulation of Pe GnRHR neurons. With regard to the hpg axis, GnRH is secreted near the pituitary portal vasculature. There, the blood flows from the median eminence to the pars anterior, where the venous drainage carries the hormones into general circulation (Wislocki 1937, 1938). Capillary connections between the median eminence and the Pe exist and have been proposed to serve as the basis for a short-loop feedback of hormones (Page 1982; Page et al. 1978). GnRHR neuron activity in the Pe follows the occurrence of a GnRH surge. We therefore considered the possibility that blood vessels could serve as a GnRH source and analyzed the relationship between CD31-marked capillaries and GFP-tagged GnRHR neurons (Fig. 5, *C–E*). Potential contact points between GnRHR neurons and Pe capillaries up to a depth of ~25 μm were examined (Fig. 5*C*). In 10 coronal slices from four females, we counted 49 GnRHR neurons within a $52 \cdot 10^6$ μm^3 Pe area, or 1 GnRHR neuron per 10^6 μm^3 Pe. The magnifications (Fig. 5*D*) illustrate that GnRHR neurons (43 out of 49) are apposed to blood capillaries (<0.3 μm), with either their somata (26 out of 110 sites, 24%) or their extensions (84 out of 110 sites, 76%). Some GnRHR somata have multiple appositions nestled in a T-junction of the capillaries. On average, we observed one soma and two GnRHR extensions per GnRHR neuron at a distance <0.3 μm from a capillary (Fig. 5*E*), whereby appositions to the GFP-tagged extension were counted only if they could be traced back to an existing soma. The majority of capillary walls in the brain are of the continuous type, with tight junctions and a continuous basement membrane (Fig. 5*F*) that forms a physical barrier against the passage of various substances. Thus an apposition between GnRHR neurons and capillaries would not make obvious sense unless specialized transporters were present. Interestingly, in addition to classical capillaries, we found capillaries with endothelial cells containing many caveaolae-like structures in the periventricular area (Fig. 5, *G* and *I*), suggesting a less constrained BBB in this region of the central nervous system. Fenestrated capillaries with discontinuous BBB, as are present in the median eminence, were not observed (Fig. 5, *H* and *J*). Communication between capillaries and neurons does not necessarily indicate open access from the blood to the brain. Furthermore, the 3V as a source for GnRH should be kept in mind (Rodriguez et al. 2010).

Systemic cetrorelix treatment mimics proestrus firing in Pe GnRHR neurons. A less constrained BBB in the periventricular area led us to consider whether in vivo treatment with the GnRHR antagonist cetrorelix, which is known to block GnRH/GnRHR signaling mainly at the level of the gonadotropes, and which is therefore used in reproductive therapies and hormone-dependent diseases, could also affect the activity of GnRHR neurons in the brain. Cetrorelix treatment causes an immediate inhibition of gonadotropins by blocking GnRHR in the pitu-

Fig. 3. Gonadotropin-releasing hormone (GnRH) induces a switch in the action potential activity of GnRHR neurons. *A*: example of an individual GnRHR neuron responding to a 1-s pulse of 0.5 nM GnRH with an increase in extracellularly recorded action-potential-driven, capacitive currents in the presence of a cocktail of synaptic blockers (pipette potential, 0 mV). *B*: GnRH increased the spike frequency in all GnRHR neurons tested, compared with control stimulation (gray dots connected by dashed lines). Control, 5.0 ± 1.3 Hz ($n = 4$); GnRH, 6.8 ± 1.3 Hz ($n = 4$). Paired *t*-test t(3) = 3.59, $^*P < 0.05$. *C–E*: GnRH-induced membrane depolarization and rise in action potential frequency in GnRHR neurons (current-clamp recording in the presence of synaptic blockers). *C*: example of an individual GnRHR neuron stimulated with either control or 1 nM GnRH (1-s pulse). GnRH stimulation induced an initial action potential burst, followed by a sustained elevation in membrane potential (4.8 mV in this example). *D*: histogram summarizing the mean change in membrane potential (ΔV) induced by either control or GnRH stimulation within the first 10 s following stimulation. Control, −0.3 ± 0.5 mV; GnRH, 1.5 ± 0.5 mV. Paired *t*-test t(4) = −4.14, $^*P < 0.05$. *E*: spike frequency index demonstrating the rise in spike frequency following GnRH stimulation. Paired *t*-test t(4) = −2.81, $^*P < 0.05$. *F–H:* voltage-clamp recordings of GnRHR neurons in the presence of synaptic blockers and TTX at a holding potential of −60 mV. *F*: application of GnRH (10 nM) results in an inward current. *G*: Gaussian fits of averaged (solid line, $n = 5$) current frequency distributions in control (gray lines, $\mu = 0.2 \pm 0.1$ pA), and 10 nM GnRH (black lines, $\mu = -2.4 \pm 0.02$ pA). Raw data used to produce the averages (50 s before and after the start of the stimulation) are shown as dashed lines. *H*: histogram summarizing the mean current under both experimental conditions (control and 10 nM GnRH) during a period of 50 s after the start of the stimulation. Control, 0.12 ± 0.67 pA; GnRH, −2.16 ± 0.94 pA. Paired *t*-test t(4) = 3.22, $^*P < 0.05$. *I*: raster plot and corresponding perievent histograms (bin size 1 s) of extracellularly recorded, action-potential-driven, capacitive currents to 1-s pulses of either control or GnRH in the absence of synaptic blockers (pipette potential 0 mV). *J*: the mean spike frequency increased with increasing GnRH concentration, giving a $K_{1/2}$ value of 0.62 ± 0.13 nM and a Hill coefficient of 1.2 ± 0.3. ANOVA $F_{4,74} = 2.15$, $P < 0.01$. *K*: the first-spike latency decreases with increasing GnRH concentration, having a $K_{1/2}$ value of 0.61 ± 0.43 nM and a Hill coefficient of −1.9 ± 1.7. ANOVA $F_{4,74} = 2.64$, $P < 0.05$. *L*: example recording of an extracellularly recorded, action-potential-driven capacitive current of a tonic GnRHR neuron from an early proestrus female mouse stimulated with a 1-s pulse of 1 nM GnRH, revealing a dramatic change in the spike firing of the GnRHR neurons occurring ~10 s following stimulation (pipette potential 0 mV). *M*: the cumulative variance in instantaneous spike frequency (VARiF) of the GnRHR neuron shown in *L* is plotted vs. time. The GnRH-induced change in VARiF can be visualized by the shift in the cumulative VARiF slope, allowing determination of the latency and duration of this long-lasting conversion in spike activity. The original recording is positioned above the cumulative VARiF plot. *N* and *O*: dose dependency of the duration (*N*) and latency (*O*) of the long-lasting conversion in spike activity. Both values rise with increasing GnRH concentration, giving $K_{1/2}$ values and Hill coefficients of 0.48 ± 0.11 nM, 1.5 ± 0.4 (latency, mean ± SD); and 0.46 ± 0.17 nM, 1.6 ± 0.7 (duration, mean ± SD), respectively. ANOVA: latency, $F_{3,36} = 36.35$, $P < 0.0001$; duration, $F_{3,36} = 11.24$, $P < 0.0001$. *P*: extracellularly recorded, action-potential-driven capacitive current traces of a GnRHR neuron from an early proestrus female taken at various times after starting bath perfusion of 10 nM GnRH. The burst detection pattern is illustrated below the original recording using an automated unbiased process (see MATERIALS AND METHODS). The pipette potential was 0 mV. *Q*: GnRH-induced change in the spike activity from the example shown in *P*. Percentage of spikes in bursts (PSiB) and the coefficient of variation of the interspike interval (CV_{ISI}) values of the spike activity were determined every 4 min and plotted in a two-dimensional space (also see Fig. 2 and the main text). Contingent on threshold values for CV_{ISI} and PSiB (dashed lines), the neuron can be categorized as firing tonically (*blue*), and this changes to a burst pattern (*yellow*) during GnRH stimulation. *R* and *S:* bar histograms of the mean spike frequency (*R*) [pre, 3.5 ± 0.3 Hz; post, 1.4 ± 1.1 Hz; paired *t*-test t(5)=4.69, $^{**}P < 0.01$] and CV_{ISI} (*S*) [pre, 0.55 ± 0.24; post, 1.9 ± 0.8 Hz; paired *t*-test t(5)=4.38, $^{**}P < 0.01$] 4 min before the start (pre) and during the final 4 min of GnRH treatment (post) in GnRHR neurons. All dose-response curves are fits of the Hill equation in combination with an iterative Levenberg-Marquardt nonlinear, least-squares fitting routine (χ^2-test $P = 0.99$). The number of recordings is plotted in brackets above each bar.

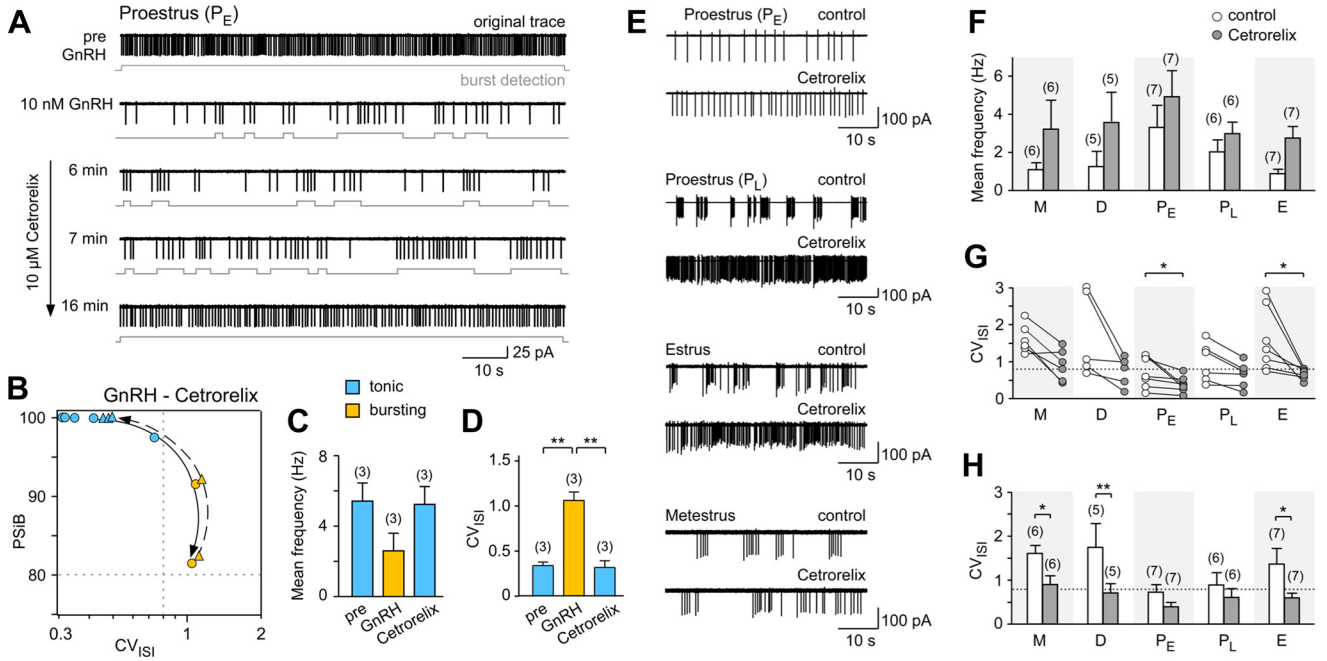

Fig. 4. Cetrorelix reverses the switch in the action potential activity of GnRHR neurons. *A*: extracellularly recorded, action-potential-driven capacitive current traces of a GnRHR neuron from a female mouse in early proestrus taken at various times after starting a bath perfusion of 10 nM GnRH, followed by 10 μM cetrorelix, a GnRHR antagonist. The burst detection pattern is depicted below the original recording using an automated unbiased process (see MATERIALS AND METHODS). The pipette potential was 0 mV. *B*: a plot of PSiB vs. CV_{ISI} (determined every 4 min) illustrates the transformation of spike activity in the GnRHR neuron shown in *A*. Contingent on threshold values for CV_{ISI} and PSiB (*gray dashed lines*), the neuron can be categorized as firing tonically (*blue*) or in a burst pattern (*yellow*). Thus GnRH stimulation converts the tonically firing neuron into a burster (*solid arrow*), an effect that is reversed by cetrorelix (*dashed arrow*). *C* and *D:* bar histograms of the mean spike frequency (*C*) and CV_{ISI} (*D*) 4 min prior to treatment (pre) and during the final 4 min of the GnRH and cetrorelix perfusion of the GnRHR neurons. Mean spike frequency: pre, 5.4 ± 1.8 Hz; GnRH, 2.6 ± 1.7 Hz; cetrorelix, 5.2 ± 1.7 Hz (ANOVA $F_{2,8} = 6.82$, $P = 0.051$); CV_{ISI}: pre, 0.34 ± 0.07 Hz; GnRH, 1.1 ± 0.16 Hz; cetrorelix, 0.32 ± 0.13 Hz (ANOVA $F_{2,8} = 1.186$, $P < 0.01$; Tukey's test $^{**}P < 0.01$). *E–H*: cetrorelix inhibits action potential burst activity. *E*: extracellularly recorded, action-potential-driven capacitive current traces of GnRHR neurons before (control) and after 10 min of treatment with cetrorelix (10 μM) in female mice at various reproductive stages. *F–H*: bar histograms of the mean spike frequency (*F*), change in CV_{ISI} of individual neurons (*G*) (Wilcoxon test $^{*}P < 0.05$), and CV_{ISI} summary as a bar histogram (*H*) (ANOVA $F_{9,50} = 3.958$, $P < 0.001$; least significant difference $^{*}P < 0.5$, $^{**}P < 0.01$) before (control, *white bars/symbols*) and after cetrorelix treatment (*gray bars/symbols*) for the various reproductive stages (metestrus, M; diestrus, D; early proestrus, P_E; late proestrus, P_L; estrus, E). The number of recordings is plotted in brackets above each bar.

itary, thereby also reducing the rate of ovulation (Duijkers et al. 1998; Reissmann et al. 2000). To test whether systemic subcutaneous cetrorelix treatment is capable of influencing the GnRH/GnRHR signaling of Pe neurons, we injected 0.9% sodium chloride (sham-treatment group), or 10 μg or 50 μg of cetrorelix into mice daily for 9 days, starting at either metestrus or diestrus for all groups (Fig. 6). Before and during the treatment, the estrous cycle stage was determined using vaginal cytology. All females cycled regularly prior to treatment and animals in the sham treatment group continued to do so during application, reaching metestrus on *day 9* in all but one case. In contrast, cetrorelix-treated females displayed impaired reproductive cycles, remaining largely in proestrus (Fig. 6*A*). To demonstrate that cetrorelix induces an effective blockade of the hpg axis and, indirectly GnRHR, we determined the ratio of the uterus to body mass and the number of tertiary/preovulatory follicles and corpora lutea (Oboti et al. 2014) in sham, cetrorelix-treated, and proestrus females. Relative uterus weight increased with cetrorelix treatment compared with the sham-treated group but was indistinguishable from untreated proestrus females, substantiating the data obtained from vaginal secretions (Fig. 6*B*). Furthermore, the ovarian tissue from the various treatment groups showed that cetrorelix application was effective in blocking GnRH-induced gonadotropin release due to an increase in the number of tertiary/preovulatory follicles, typically predicted for proestrus females, as well as a simultaneous reduction in the presence of corpora lutea (Fig. 6, *C–E*).

Cetrorelix has been reported to marginally penetrate the BBB at doses of approximately 1 to 10 μg (Schwahn et al. 2000; Telegdy et al. 2009). However, it was unclear whether 50 μg of cetrorelix crosses the BBB and directly targets GnRHR neurons. Interestingly, we found that the mean spike firing frequency of GnRH neurons increased in the cetrorelix-treated groups compared with that in the sham-treated females (Fig. 6*F*), but only the 50-μg cetrorelix application caused a significant change in spike firing, with a CV_{ISI} <0.8 (Fig. 6*G*, LSD $P < 0.001$), causing classification of these neurons as tonically firing. The distribution of tonic and bursting GnRHR neurons in the sham-treated and two cetrorelix treatment groups indicates that the number of tonically firing neurons rises with increasing cetrorelix concentration (Fig. 6*H*), reaching similar distributions as in P_E at 50 μg cetrorelix (Fig. 2*F*). A concentration of 10 μg cetrorelix appears to be below the threshold for appreciable modulation of Pe neuron activity (Fig. 6*G*, LSD $P = 0.18$), although a significant effect of cetrorelix was detected at the level of the ovaries (Fig. 6, *D* and *E*). As previously reported (Duijkers et al. 1998; Reissmann et al. 2000), and as is evident in the number of preovulatory follicles and corpora lutea per ovary (Fig. 6, *D* and *E*), treatment with 10 and 50 μg cetrorelix similarly inhibited gonadotropin release in the pituitary (LSD $P = 0.73$ and 0.94,

respectively). Therefore, systemic application of higher doses of cetrorelix influences GnRHR neuron activity and thus brain function.

DISCUSSION

GnRH is a key regulator of reproductive function in all vertebrates and has been shown to act on gonadotrope cells in the pituitary gland via the hpg axis. In addition, GnRH has been found to act as a modulator of neuronal activity in the brain. By analyzing GnRH function in genetically identified GnRHR neurons from the Pe of female mice, our research shows that the action potential firing of GnRHR neurons cyclically alternates in synchrony with the estrous cycle and that the mode of activity of the neurons switches from tonic to burst firing depending on the presence of GnRH. Our results also demonstrate that GnRHR activity during late proestrus and estrus is the main trigger for burst firing. Furthermore, we provide evidence that in vivo treatment with a well-established GnRHR antagonist, cetrorelix, which has been thought to block GnRH/GnRHR signaling mainly at the level of the gonadotropes, is also capable of affecting the activity of GnRHR neurons in the brain.

GnRH induces burst firing in hypothalamic Pe GnRHR neurons. GnRH stimulation triggers the conversion of the mode of activity of GnRHR neurons from tonic to burst firing, an effect that can be reversed by blocking GnRHR. Before the firing pattern of GnRHR neurons underwent the GnRH-induced switch, the neurons showed a rise in spike frequency and an extended elevation of the membrane potential, indicating that GnRH activates a depolarizing conductance in these Pe neurons. The first-spike latency, which may contribute temporal information regarding the detection of the stimulus, decreased significantly from 340 to 60 ms with increasing GnRH concentration. Other metabotropic receptor-coupled signal transduction cascades show latencies ranging from 7 ms in phototransduction (Cobbs and Pugh 1987; Hestrin and Korenbrot 1990) up to 150–300 ms in olfaction (Firestein et al. 1990; Leinders-Zufall et al. 1998). The difference in response latency obviously reflects the speed of the signaling cascade linking the GPCR to its effector proteins and the ion channels that ultimately modify the membrane potential. However, the mechanism by which GnRH modulates and triggers the action po-

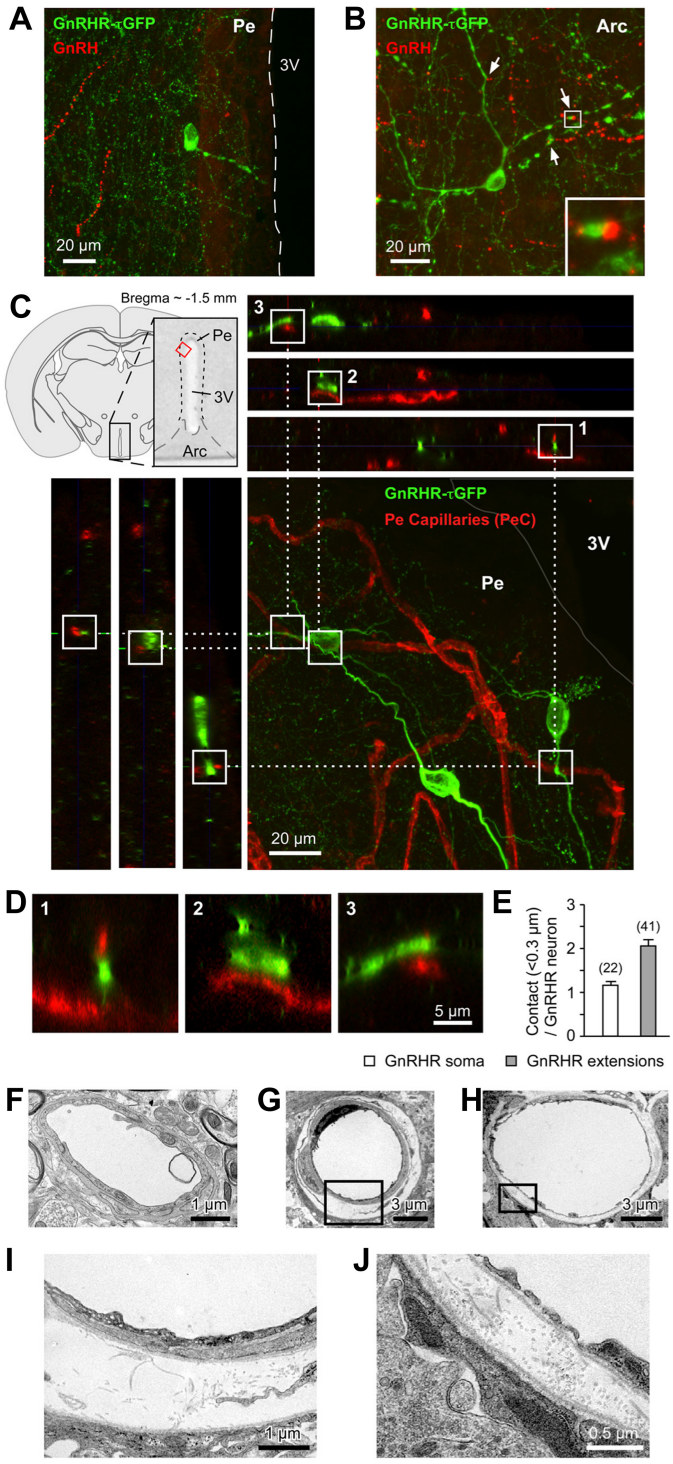

Fig. 5. GnRHR neurons have multiple close appositions with capillaries. *A*: confocal image of a coronal brain slice (bregma −0.82) showing a green fluorescent protein (GFP)-positive GnRHR-expressing neuron (green) and GnRH-expressing fibers (red) in the periventricular hypothalamic nucleus (Pe). No potential contact points (appositions) between these structures were observed (n = 26, 3 female mice). The dashed line indicates the border between the Pe and the third ventricle (3V). *B*: GnRHR neurons of the arcuate nucleus (bregma −1.58) possess various appositions (<0.3 μm) per identified GnRHR neuron (n = 5, 3 female mice). *Inset*: higher magnification of the apposition indicated by the white box. Arrows indicate appositions identified using transverse confocal sectioning. *C*: confocal images of a coronal brain slice showing GFP-positive GnRHR expressing neurons (green) and Pe capillaries (red) in the Pe. *Top left*: overview and higher magnification of a coronal brain slice showing the location of the Pe and arcuate nucleus (Arc) of the hypothalamus next to the 3V. Optical *xyz*-sections (*right lower*) were merged to obtain a high-resolution *xy*-image with a thickness of 20 μm. The location and perimeter of the 3V is indicated in gray. Transverse confocal sections (*top*, *xz*; *left*, *yz*) allowed examination of appositions (white boxes) between GnRHR neurons and Pe capillaries. *D*: regions indicated by the numbered white boxes in *C* at higher magnification (*xz*-plane) show the close apposition of GnRHR fibers (*1*, *3*) and a soma (*2*) to the Pe capillaries. *E*: number of appositions between capillaries and GFP-marked soma or extensions per GnRHR neuron. Appositions of a GFP-tagged extension were counted only when the soma of the GnRHR neuron could be identified and was located within the Pe. *F–J*: electron micrographs of the different capillary types present in the hypothalamus. Both the classical continuous, nonfenestrated brain capillary (*F*) and capillaries in which endothelial cells contain numerous vesicular structures that look like caveolae (*G* and *I*) were detected in the periventricular area. Similar to those observed in the median eminence (*H* and *J*), these capillaries have a widened, translucent perivascular space. Fenestrated capillaries (*H* and *J*) were found only in the area of the median eminence. The black boxes in *G* and *H* are magnified in *I* and *J*, respectively.

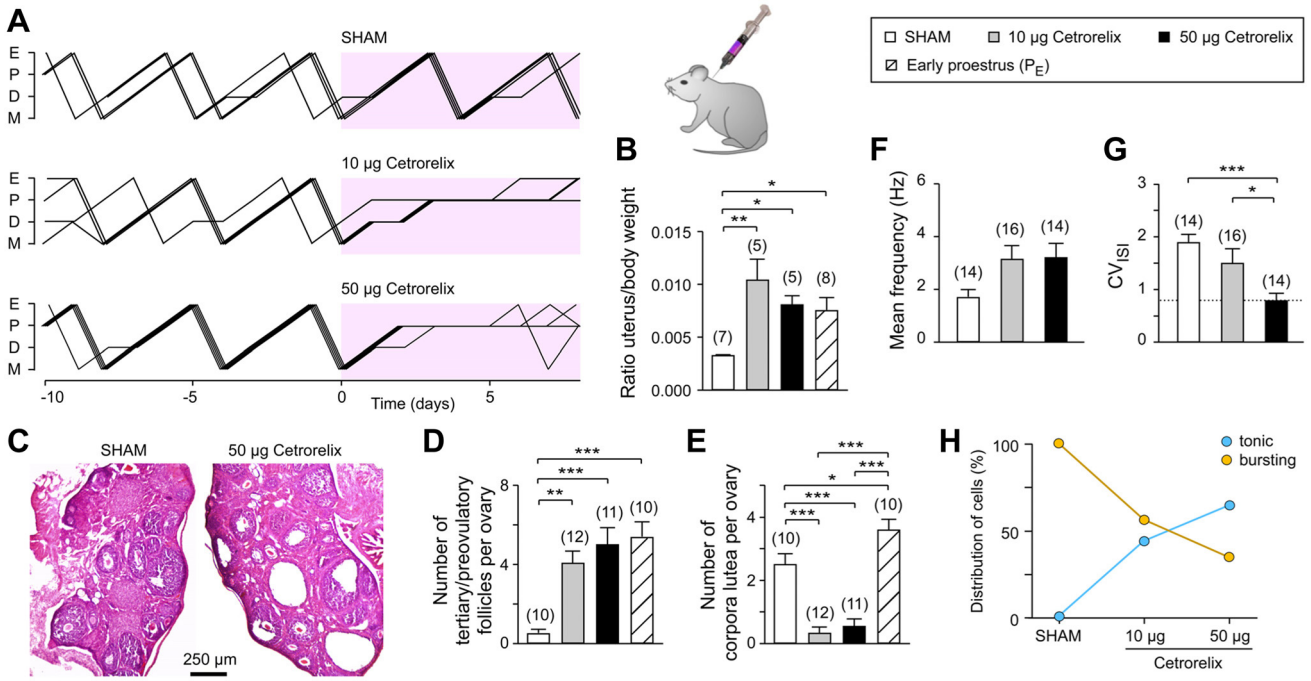

Fig. 6. In vivo cetrorelix treatment modulates the reproductive cycle and GnRHR neuron activity in the Pe. *A*: plot of the estrous cycle of GRIC/eR26-τGFP mice (at least five females per treatment group) demonstrating a normal 4- to 5-day cycle length prior to the start of subcutaneous application (t = 0 days) of either 10 or 50 μg cetrorelix for 9 days. Sham-treated females continued their normal reproductive cycles, in contrast to the cetrorelix-treated groups. *B*: uterus weight increased following cetrorelix treatment compared with the sham-treatment group but was indistinguishable from females in early proestrus. ANOVA $F_{3,16} = 4.754$, $P < 0.01$; Tukey's test $^*P < 0.5$, $^{**}P < 0.01$. The number of mice is plotted in brackets above each bar. *C*: effect of cetrorelix on the morphological appearance of the mouse ovary. Sections taken from sham-treated mice and those treated with 50 μg cetrorelix. *D*: ovaries of cetrorelix-treated mice and females in early proestrus reveal high numbers of tertiary and preovulatory follicles compared with the sham-treated group. ANOVA $F_{3,39} = 10.70$, $P < 0.0001$; Tukey's test $^{**}P < 0.01$, $^{***}P < 0.001$. *E*: cetrorelix application reduced the presence of corpora lutea compared with sham-treated females and those in early proestrus. ANOVA $F_{3,39} = 31.99$, $P < 0.0001$; Tukey's test $^*P < 0.05$, $^{**}P < 0.01$, $^{***}P < 0.001$. The number of mice is plotted in brackets above each bar. *F* and *G*: bar histograms of the mean spike frequency (*F*) (ANOVA $F_{2,41} = 3.037$, $P = 0.06$) and the CV_{ISI} (*G*) (ANOVA $F_{2,41} = 6.556$, $P < 0.01$; Tukey's test $^*P < 0.05$, $^{***}P < 0.001$) of GnRHR neurons during sham treatment, and 10 μg and 50 μg cetrorelix applications. The number of neurons is plotted in brackets above each bar. *H*: plot of the distribution of all GnRHR neurons firing either tonically (*blue*) or in bursts (*yellow*) by subcutaneous treatment group (sham treatment $n = 14$, 10 μg cetrorelix $n = 16$, 50 μg cetrorelix $n = 14$).

tential pattern in a concentration-dependent manner remains unknown. Although GnRH is known to act via the $G_{q/11}$-coupled GnRHR to activate phospholipase C, resulting in the mobilization of Ca^{2+}, the involvement of other second-messenger pathways as well as G-proteins has also been proposed (Cohen-Tannoudji et al. 2012; Naor and Huhtaniemi 2012). Using Ca^{2+} imaging, we have observed two types of somatic Ca^{2+} transients in Pe GnRHR neurons that show a 25-s delay between the responses at saturating GnRH (Wen et al. 2011). The latency of the GnRH-induced long-lasting change in spike activity was observed in a similar range (Fig. 5), indicating a role for Ca^{2+} in adjusting the action potential activity pattern for these neurons. Further experiments are needed to clarify the involvement of the signal transduction pathways in regulating Pe GnRHR neuron activity.

Endogenous GnRH acting on GnRHR as the main trigger for burst firing. Inhibiting the GnRHR with its antagonist cetrorelix was sufficient to convert burst firing into tonic firing during the preovulatory period, indicating that the activity of the receptor itself triggers the transformation in action potential firing in Pe neurons. Cetrorelix also significantly inhibited the activity in GnRHR neurons during metestrus and diestrus but could not cause the complete shift to tonic firing, possibly because of the involvement of other hormones or synaptic input from adjacent neurons. Hypothalamic GnRH is released in pulses that increase in frequency and intensity during late proestrus (Radovick et al. 2012; Sisk et al. 2001). Estradiol levels rise during the estrous cycle, peaking during proestrus (Butcher et al. 1974), and differentially affecting GnRH-secreting neurons (Abe and Terasawa 2005; Chu et al. 2009). GnRH secretion decreases in the presence of low estradiol concentration but is augmented at high concentrations. Interestingly, the increase in the number of tonically firing GnRHR neurons can be correlated with estradiol levels during the estrous cycle (Fig. 2*F*), suggesting that decreased GnRH release due to estradiol alleviates GnRHR neuronal burst activity. The direct effect of the estradiol-generated tonicity of GnRHR neuron firing could result from the prevention of intrinsic cascades known to induce oscillatory spike behavior (Bal et al. 1995; Chu et al. 2010) or by the modulation of local network activity by estradiol (Christian and Moenter 2007; Veliskova and Velisek 2007). Estradiol is well known as an initiator of burst activity (Abe and Terasawa 2005; Chu et al. 2009), but such a scenario seems unlikely here. The number of bursting neurons decreases (Fig. 2*F*) with a reported increase in estradiol levels (Butcher et al. 1974). In addition, non-proestrus GnRHR neurons firing in bursts can be converted to tonically firing neurons with the help of a GnRH antagonist. Likewise, originally, tonically firing neurons in early proestrus that have been prestimulated with GnRH and that are therefore firing in bursts will reverse their activity in the presence of the antagonist, indicating that GnRHR activation causes the change in spike activity. Further-

more, we were unable to detect estrogen receptor-α (ERα) expression in GnRHR neurons of the Pe (V. Periasamy and U. Boehm, unpublished observation), arguing against a genomic estrogen effect in these cells. Estrogen might, however, act on adjacent cells that do express ERα to modulate GnRHR neurons. Disrupting the local network with synaptic blockers (Fig. 2*I*) indicates that hormone-dependent network pathways may indeed influence the activity of GnRHR neurons during metestrus, diestrus, and early proestrus when estradiol is rising. Progesterone is another steroid hormone associated with the control of GnRH secretion (Bashour and Wray 2012) and is therefore a candidate for the modulation of GnRHR neuron activity. Both estrogen and progesterone levels might be needed to prime GnRHR neurons during proestrus for the spike code activity to switch to tonic firing, thus preparing them to respond to the heightened activity of the GnRH/LH pulse generator. Alternatively, agonist-induced GnRHR internalization (Finch et al. 2009) could be argued as the cause for the increased presence of tonically firing neurons during early proestrus and the reduction in GnRHR activity-induced spike bursting behavior in Pe neurons. However, this possibility can be excluded because a GnRH upsurge must be present to induce the process. Receptor desensitization can also be ruled out because type I mammalian GnRHR, which is the only GnRH receptor found in mice (Reinhart et al. 1992; Stewart et al. 2009), does not desensitize through the lack of arrestin binding (Finch et al. 2009; Naor and Huhtaniemi 2012). Currently, our data support a modulation of GnRHR neurons in the periventricular nucleus by the network during metestrus, diestrus, and early proestrus, followed by a switch in action potential firing initiated by GnRH during the late phase of proestrus. However, GnRHR neurons located in other brain areas may not necessarily depend on GnRH linked to the reproductive cycle and could be influenced by variations in gonadal steroids or other hormones.

In vivo modulation of GnRH/GnRHR signaling in the brain. Cetrorelix treatment efficiently inhibits gonadotropin release by blocking GnRHR in the pituitary, thereby reducing the rate of ovulation (Duijkers et al. 1998; Reissmann et al. 2000). Systemic treatment of female mice with 50 μg cetrorelix enabled us to modulate GnRHR neuron activity, with Pe neurons firing more tonically and mimicking the spike firing observed in early proestrus (see Figs. 2*F* and 6*H*). Many peptides, including GnRH, cross the BBB (Banks 2009; Barrera et al. 1991). Although cetrorelix penetrates the BBB only marginally at the previously tested doses of approximately 1–10 μg (Schwahn et al. 2000; Telegdy et al. 2009), higher cetrorelix concentrations might be able to pass through the BBB. Subcutaneous 50 μg cetrorelix treatment affected GnRHR neuron activity, providing support for the proposal that therapeutic drugs similar to cetrorelix might be able to gain access to the brain and modulate GnRHR neuron activity. Gonadal hormones such as estradiol and progesterone are also reduced during cetrorelix treatment (Duijkers et al. 1998); however, a direct effect of these hormones on GnRHR neurons is unlikely, as discussed above.

Although these lines of reasoning clearly point to endogenous GnRH as the main regulator of the change in spike activity in GnRHR neurons, the decapeptide GnRH has a reported serum half-life of only 2–6 min (Pimstone et al. 1977; Woodley 1994). This may be insufficient to induce the differential action potential pattern observed in acute slice recordings. Plasma GnRH appears to undergo rapid clearance from circulation as it is metabolized by serum and liver peptidases, leading to the loss of biological activity. *GnRH* mRNA levels have a half-life of 22–30 h (Gore and Roberts 1997). If GnRH-secreting fibers remain active even after they have been severed from their cell bodies, they may still release GnRH into the vascular system or 3V. On the other hand, GnRH could be stable for an extended period in the brain. Human patients with liver or renal dysfunction have GnRH serum half-lifes of up to 20 min (Pimstone et al. 1977), indicating that the plasma GnRH level depends on the degradation and clearance of GnRH.

One protocol for in vitro fertilization uses the working principle of the hpg axis for the regulation of oocyte maturation and ovulation by adding a bolus of GnRH agonist during prolonged cotreatment with a GnRH antagonist (Kol and Humaidan 2013). The GnRH agonist displaces the antagonist in the pituitary, thereby reactivating the GnRHR and resulting in a gonadotropin surge. As our data of systemic cetrorelix treatment in mice suggest, GnRH agonist/antagonist actions may not be restricted to the pituitary and could potentially have undesirable side effects by acting on GnRHR-expressing neurons in multiple brain areas (Badr and Pelletier 1987; Jennes et al. 1997; Wen et al. 2011). Therefore, a detailed analysis of the functional activity of GnRHR neurons in various brain regions will be essential to achieve a complete understanding of the central control of reproduction by the mammalian brain.

ACKNOWLEDGMENTS

We thank personnel with the SFB 894-P1 project for the use of the Zeiss confocal microscope; Sarah Boll and Gabi Kiefer for excellent technical assistance; Martina Pyrski and Lique Coolen for stimulating discussions; and Michael Candlish and, in particular, Frank Zufall, for comments on earlier versions of the manuscript.

GRANTS

Support for this study was provided by a Volkswagen Foundation grant to T. Leinders-Zufall; and by Deutsche Forschungsgemeinschaft Grants SPP 1392 to T. Leinders-Zufall and U. Boehm; SFB 894 to F. Schmitz, T. Leinders-Zufall, and U. Boehm; and BO1743/2 to U. Boehm. T. Leinders-Zufall is a Lichtenberg Professor of the Volkswagen Foundation.

DISCLOSURES

No conflicts of interest, financial or otherwise, are declared by the authors.

AUTHOR CONTRIBUTIONS

U.B. and T.L.-Z. conception and design of research; C.S., T.T., H.P., T.B., S.P., and F.S. performed experiments; C.S., T.T., H.P., T.B., S.P., F.S., and T.L.-Z. analyzed data; C.S., T.T., H.P., T.B., F.S., and T.L.-Z. interpreted results of experiments; C.S., T.T., H.P., T.B., F.S., and T.L.-Z. prepared figures; C.S., T.T., T.B., F.S., and T.L.-Z. drafted manuscript; U.B. and T.L.-Z. edited and revised manuscript; C.S., T.T., H.P., T.B., S.P., O.M., F.S., U.B., and T.L.-Z. approved final version of manuscript.

REFERENCES

Abe H, Terasawa E. Firing pattern and rapid modulation of activity by estrogen in primate luteinizing hormone releasing hormone-1 neurons. *Endocrinology* 146: 4312–4320, 2005.

Badr M, Pelletier G. Characterization and autoradiographic localization of LHRH receptors in the rat brain. *Synapse* 1: 567–571, 1987.

Bal T, von Krosigk M, McCormick DA. Role of the ferret perigeniculate nucleus in the generation of synchronized oscillations in vitro. *J Physiol* 483, *Pt* 3: 665–685, 1995.

Banks WA. Characteristics of compounds that cross the blood-brain barrier. *BMC Neurol* 9, *Suppl* 1: S3, 2009.

Barran PE, Roeske RW, Pawson AJ, Sellar R, Bowers MT, Morgan K, Lu ZL, Tsuda M, Kusakabe T, Millar RP. Evolution of constrained gonadotropin-releasing hormone ligand conformation and receptor selectivity. *J Biol Chem* 280: 38569–38575, 2005.

Barrera CM, Kastin AJ, Fasold MB, Banks WA. Bidirectional saturable transport of LHRH across the blood-brain barrier. *Am J Physiol Endocrinol Metab* 261: E312–E318, 1991.

Bashour NM, Wray S. Progesterone directly and rapidly inhibits GnRH neuronal activity via progesterone receptor membrane component 1. *Endocrinology* 153: 4457–4469, 2012.

Butcher RL, Collins WE, Fugo NW. Plasma concentration of LH, FSH, prolactin, progesterone and estradiol-17β throughout the 4-day estrous cycle of the rat. *Endocrinology* 94: 1704–1708, 1974.

Caligioni CS. Assessing reproductive status/stages in mice. *Curr Protoc Neurosci* 48: 1–8, 2009.

Caraty A, Skinner DC. Gonadotropin-releasing hormone in third ventricular cerebrospinal fluid: endogenous distribution and exogenous uptake. *Endocrinology* 149: 5227–5234, 2008.

Christian CA, Moenter SM. Estradiol induces diurnal shifts in GABA transmission to gonadotropin-releasing hormone neurons to provide a neural signal for ovulation. *J Neurosci* 27: 1913–1921, 2007.

Chu Z, Andrade J, Shupnik MA, Moenter SM. Differential regulation of gonadotropin-releasing hormone neuron activity and membrane properties by acutely applied estradiol: dependence on dose and estrogen receptor subtype. *J Neurosci* 29: 5616–5627, 2009.

Chu Z, Takagi H, Moenter SM. Hyperpolarization-activated currents in gonadotropin-releasing hormone (GnRH) neurons contribute to intrinsic excitability and are regulated by gonadal steroid feedback. *J Neurosci* 30: 13373–13383, 2010.

Cobbs WH, Pugh EN Jr. Kinetics and components of the flash photocurrent of isolated retinal rods of the larval salamander, *Ambystoma tigrinum*. *J Physiol* 394: 529–572, 1987.

Cohen-Tannoudji J, Avet C, Garrel G, Counis R, Simon V. Decoding high gonadotropin-releasing hormone pulsatility: a role for GnRH receptor coupling to the cAMP pathway? *Front Endocrinol (Lausanne)* 3: 107, 2012.

Conn PM, Hazum E. Luteinizing hormone release and gonadotropin-releasing hormone (GnRH) receptor internalization: independent actions of GnRH. *Endocrinology* 109: 2040–2045, 1981.

Cottrell GT, Ferguson AV. Sensory circumventricular organs: central roles in integrated autonomic regulation. *Regul Pept* 117: 11–23, 2004.

Duijkers IJ, Klipping C, Willemsen WN, Krone D, Schneider E, Niebch G, Hermann R. Single and multiple dose pharmacokinetics and pharmacodynamics of the gonadotrophin-releasing hormone antagonist Cetrorelix in healthy female volunteers. *Hum Reprod* 13: 2392–2398, 1998.

Dyer RG, Dyball RE. Evidence for a direct effect of LRF and TRF on single unit activity in the rostral hypothalamus. *Nature* 252: 486–488, 1974.

Finch AR, Caunt CJ, Armstrong SP, McArdle CA. Agonist-induced internalization and downregulation of gonadotropin-releasing hormone receptors. *Am J Physiol Cell Physiol* 297: C591–C600, 2009.

Firestein S, Shepherd GM, Werblin FS. Time course of the membrane current underlying sensory transduction in salamander olfactory receptor neurones. *J Physiol* 430: 135–158, 1990.

Gore AC. *GnRH: The master molecule of reproduction*. Norwell, MA: Kluwer Academic Publishers, 2002.

Gore AC, Roberts JL. Regulation of gonadotropin-releasing hormone gene expression in vivo and in vitro. *Front Neuroendocrinol* 18: 209–245, 1997.

Halmos G, Schally AV, Pinski J, Vadillo-Buenfil M, Groot K. Down-regulation of pituitary receptors for luteinizing hormone-releasing hormone (LH-RH) in rats by LH-RH antagonist Cetrorelix. *Proc Natl Acad Sci USA* 93: 2398–2402, 1996.

Herde MK, Geist K, Campbell RE, Herbison AE. Gonadotropin-releasing hormone neurons extend complex highly branched dendritic trees outside the blood-brain barrier. *Endocrinology* 152: 3832–3841, 2011.

Hestrin S, Korenbrot JI. Activation kinetics of retinal cones and rods: response to intense flashes of light. *J Neurosci* 10: 1967–1973, 1990.

Jennes L, Eyigor O, Janovick JA, Conn PM. Brain gonadotropin releasing hormone receptors: localization and regulation. *Recent Prog Horm Res* 52: 475–490; discussion 490–491, 1997.

Kol S, Humaidan P. GnRH agonist triggering: recent developments. *Reprod Biomed Online* 26: 226–230, 2013.

Leinders-Zufall T, Cockerham RE, Michalakis S, Biel M, Garbers DL, Reed RR, Zufall F, Munger SD. Contribution of the receptor guanylyl cyclase GC-D to chemosensory function in the olfactory epithelium. *Proc Natl Acad Sci USA* 104: 14507–14512, 2007.

Leinders-Zufall T, Greer CA, Shepherd GM, Zufall F. Imaging odor-induced calcium transients in single olfactory cilia: specificity of activation and role in transduction. *J Neurosci* 18: 5630–5639, 1998.

Leinders-Zufall T, Ishii T, Chamero P, Hendrix P, Oboti L, Schmid A, Kircher S, Pyrski M, Akiyoshi S, Khan M, Vaes E, Zufall F, Mombaerts P. A family of nonclassical class I MHC genes contributes to ultrasensitive chemodetection by mouse vomeronasal sensory neurons. *J Neurosci* 34: 5121–5133, 2014.

Lu ZL, Gallagher R, Sellar R, Coetsee M, Millar RP. Mutations remote from the human gonadotropin-releasing hormone (GnRH) receptor-binding sites specifically increase binding affinity for GnRH II but not GnRH I: evidence for ligand-selective, receptor-active conformations. *J Biol Chem* 280: 29796–29803, 2005.

Marder E, O'Leary T, Shruti S. Neuromodulation of circuits with variable parameters: single neurons and small circuits reveal principles of state-dependent and robust neuromodulation. *Annu Rev Neurosci* 37: 329–346, 2014.

Moss RL. Role of hypophysiotropic neurohormones in mediating neural and behavioral events. *Fed Proc* 36: 1978–1983, 1977.

Moss RL, Foreman MM. Potentiation of lordosis behavior by intrahypothalamic infusion of synthetic luteinizing hormone-releasing hormone. *Neuroendocrinology* 20: 176–181, 1976.

Moss RL, McCann SM. Induction of mating behavior in rats by luteinizing hormone-releasing factor. *Science* 181: 177–179, 1973.

Naor Z, Huhtaniemi I. Interactions of the GnRH receptor with heterotrimeric G proteins. *Front Neuroendocrinol* 34: 88–94, 2013.

Oboti L, Pérez-Gómez A, Keller M, Jacobi E, Birnbaumer L, Leinders-Zufall T, Zufall F, Chamero P. A wide range of pheromone-stimulated sexual and reproductive behaviors in female mice depend on G protein Gαo. *BMC Biol* 12: 31, 2014.

Page RB. Pituitary blood flow. *Am J Physiol Endocrinol Metab* 243: E427–E442, 1982.

Page RB, Leure-duPree AE, Bergland RM. The neurohypophyseal capillary bed. II. Specializations within median eminence. *Am J Anat* 153: 33–65, 1978.

Pawlas Z, Klebanov LB, Benes V, Prokesova M, Popelar J, Lansky P. First-spike latency in the presence of spontaneous activity. *Neural Comput* 22: 1675–1697, 2010.

Paxinos G, Franklin J. *The mouse brain in stereotaxic coordinates*. San Diego, CA: Academic Press, 2001.

Pfaff DW. Luteinizing hormone-releasing factor potentiates lordosis behavior in hypophysectomized ovariectomized female rats. *Science* 182: 1148–1149, 1973.

Pimstone B, Epstein S, Hamilton SM, LeRoith D, Hendricks S. Metabolic clearance and plasma half disappearance time of exogenous gonadotropin releasing hormone in normal subjects and in patients with liver disease and chronic renal failure. *J Clin Endocrinol Metab* 44: 356–360, 1977.

Radovick S, Levine JE, Wolfe A. Estrogenic regulation of the GnRH neuron. *Front Endocrinol (Lausanne)* 3: 52, 2012.

Reinhart J, Mertz LM, Catt KJ. Molecular cloning and expression of cDNA encoding the murine gonadotropin-releasing hormone receptor. *J Biol Chem* 267: 21281–21284, 1992.

Reissmann T, Schally AV, Bouchard P, Riethmiiller H, Engel J. The LHRH antagonist cetrorelix: a review. *Hum Reprod Update* 6: 322–331, 2000.

Robin K, Maurice N, Degos B, Deniau JM, Martinerie J, Pezard L. Assessment of bursting activity and interspike intervals variability: a case study for methodological comparison. *J Neurosci Methods* 179: 142–149, 2009.

Rodriguez EM, Blázquez JL, Guerra M. The design of barriers in the hypothalamus allows the median eminence and the arcuate nucleus to enjoy private milieus: the former opens to the portal blood and the latter to the cerebrospinal fluid. *Peptides* 31: 757–776, 2010.

Saper CB. Hypothalamus. In: *The Human Nervous System*, edited by Paxinos G and Mai JK. San Diego, CA: Academic Press, 2004, p. 513–550.

Schauer C, Leinders-Zufall T. Imaging calcium responses in GFP-tagged neurons of hypothalamic mouse brain slices. *J Vis Exp* 66: e4213, 2012.

Schmidt D, von Hochstetter AR. The use of CD31 and collagen IV as vascular markers. A study of 56 vascular lesions. *Pathol Res Pract* 191: 410–414, 1995.

Schoch S, Mittelstaedt T, Kaeser PS, Padgett D, Feldmann N, Chevaleyre V, Castillo PE, Hammer RE, Han W, Schmitz F, Lin W, Sudhof TC. Redundant functions of RIM1α and RIM2α in Ca^{2+}-triggered neurotransmitter release. *EMBO J* 25: 5852–5863, 2006.

Schwahn M, Schupke H, Gasparic A, Krone D, Peter G, Hempel R, Kronbach T, Locher M, Jahn W, Engel J. Disposition and metabolism of cetrorelix, a potent luteinizing hormone-releasing hormone antagonist, in rats and dogs. *Drug Metab Dispos* 28: 10–20, 2000.

Selinger JV, Kulagina NV, O'Shaughnessy TJ, Ma W, Pancrazio JJ. Methods for characterizing interspike intervals and identifying bursts in neuronal activity. *J Neurosci Methods* 162: 64–71, 2007.

Sisk CL, Richardson HN, Chappell PE, Levine JE. In vivo gonadotropin-releasing hormone secretion in female rats during peripubertal development and on proestrus. *Endocrinology* 142: 2929–2936, 2001.

Skinner DC, Caraty A, Malpaux B, Evans NP. Simultaneous measurement of gonadotropin-releasing hormone in the third ventricular cerebrospinal fluid and hypophyseal portal blood of the ewe. *Endocrinology* 138: 4699–4704, 1997.

Stewart AJ, Katz AA, Millar RP, Morgan K. Retention and silencing of prepro-GnRH-II and type II GnRH receptor genes in mammals. *Neuroendocrinology* 90: 416–432, 2009.

Telegdy G, Tanaka M, Schally AV. Effects of the LHRH antagonist Cetrorelix on the brain function in mice. *Neuropeptides* 43: 229–234, 2009.

Veliskova J, Velisek L. Beta-estradiol increases dentate gyrus inhibition in female rats via augmentation of hilar neuropeptide Y. *J Neurosci* 27: 6054–6063, 2007.

Wen S, Gotze IN, Mai O, Schauer C, Leinders-Zufall T, Boehm U. Genetic identification of GnRH receptor neurons: a new model for studying neural circuits underlying reproductive physiology in the mouse brain. *Endocrinology* 152: 1515–1526, 2011.

Wislocki GB. The vascular supply of the hypophysis cerebri of the cat. *Anat Rec* 69: 361–387, 1937.

Wislocki GB. The vascular supply of the hypophysis cerebri of the rhesus monkey and man. *Res Publ Assoc Res Nerv Ment Dis* 17: 48–68, 1938.

Woodley JF. Enzymatic barriers for GI peptide and protein delivery. *Crit Rev Ther Drug Carrier Syst* 11: 61–95, 1994.